2936–2948 *Nucleic Acids Research, 2016, Vol. 44, No. 6* *Published online 20 January 2016*
doi: 10.1093/nar/gkw025

Solution structure of the Z-DNA binding domain of PKR-like protein kinase from *Carassius auratus* and quantitative analyses of the intermediate complex during B–Z transition

Ae-Ree Lee[1,†], Chin-Ju Park[2,†], Hae-Kap Cheong[3], Kyoung-Seok Ryu[3], Jin-Wan Park[1,3], Mun-Young Kwon[1], Janghyun Lee[4], Kyeong Kyu Kim[5], Byong-Seok Choi[4] and Joon-Hwa Lee[1,*]

[1]Department of Chemistry and RINS, Gyeongsang National University, Gyeongnam 52828, Republic of Korea, [2]Division of Liberal Arts and Sciences and Department of Chemistry, Gwangju Institute of Science and Technology, Gwangju 61005, Republic of Korea, [3]Division of Magnetic Resonance, KBSI, Chungbuk 28119, Republic of Korea, [4]Department of Chemistry, Korea Advanced Institute of Science and Technology, Daejeon 34141, Republic of Korea and [5]Department of Molecular Cell Biology, Sungkyunkwan University School of Medicine, Gyeonggi 16419, Republic of Korea

Received August 20, 2015; Revised December 6, 2015; Accepted January 11, 2016

ABSTRACT

Z-DNA binding proteins (ZBPs) play important roles in RNA editing, innate immune response and viral infection. Structural and biophysical studies show that ZBPs initially form an intermediate complex with B-DNA for B–Z conversion. However, a comprehensive understanding of the mechanism of Z-DNA binding and B–Z transition is still lacking, due to the absence of structural information on the intermediate complex. Here, we report the solution structure of the Zα domain of the ZBP-containing protein kinase from *Carassius auratus* (caZα$_{PKZ}$). We quantitatively determined the binding affinity of caZα$_{PKZ}$ for both B-DNA and Z-DNA and characterized its B–Z transition activity, which is modulated by varying the salt concentration. Our results suggest that the intermediate complex formed by caZα$_{PKZ}$ and B-DNA can be used as molecular ruler, to measure the degree to which DNA transitions to the Z isoform.

INTRODUCTION

Left-handed Z-DNA is a higher energy conformation than B-DNA and forms under conditions of high salt, negative supercoiling and complex formation with Z-DNA binding proteins (ZBPs) (1–3). ZBPs have been identified in an RNA editing enzyme (ADAR1), DNA-dependent activator of interferon-regulatory factor (DAI, also known as DLM-1 and ZBP1), the viral E3L protein and a fish protein kinase containing a ZBP (PKZ) (Figure 1A) (4–7). The crystal structures of the Zα domains of human ADAR1 (hZα$_{ADAR1}$) (8), mouse DAI (mZα$_{DLM1}$) (5) and yatapoxvirus E3L (yabZα$_{E3L}$) (9), and *Carassius auratus* PKZ (caZα$_{PKZ}$) (10) in complex with 6-base-paired (6-bp) dT(CG)$_3$ revealed that two molecules of Zα bind to each strand of double-stranded (ds) Z-DNA, yielding 2-fold symmetry with respect to the DNA helical axis. The intermolecular interaction with Z-DNA is mediated by five residues in the α3 helix and four residues in the β-hairpin (β2-loop-β3) (Figure 1B). Among them, four residues (K34, N38, Y42 and W60; marked with asterisks in Figure 1A) show a high degree of conservation and play important roles in Zα function.

In addition, structural studies in solution suggested an *active* mechanism of B–Z transition of a 6-bp DNA induced by ZBPs, in which (i) the ZBP (denoted as **P**) binds directly to B-DNA (denoted as **B**); (ii) the B-DNA in the complex is converted to Z-form; and (iii) the stable **ZP$_2$** complex (the Z-form DNA denoted as **Z**) is produced by the addition of another **P** to **ZP** (Figure 1C) (11). In spite of these extensive structural studies (5,8–10), the detailed molecular mechanism of DNA binding and B–Z transition is still unclear due to the lack of structural data on the intermediate complexes. Therefore it is crucial to obtain structural snapshots and/or quantitative analyses of each step in the B–Z transition: B-DNA binding complex, transition complex and Z-DNA binding complex.

*To whom correspondence should be addressed. Tel: +82 55 772 1490; Fax: +82 55 772 1490; Email: joonhwa@gnu.ac.kr
†These authors contributed equally to the paper as first authors.

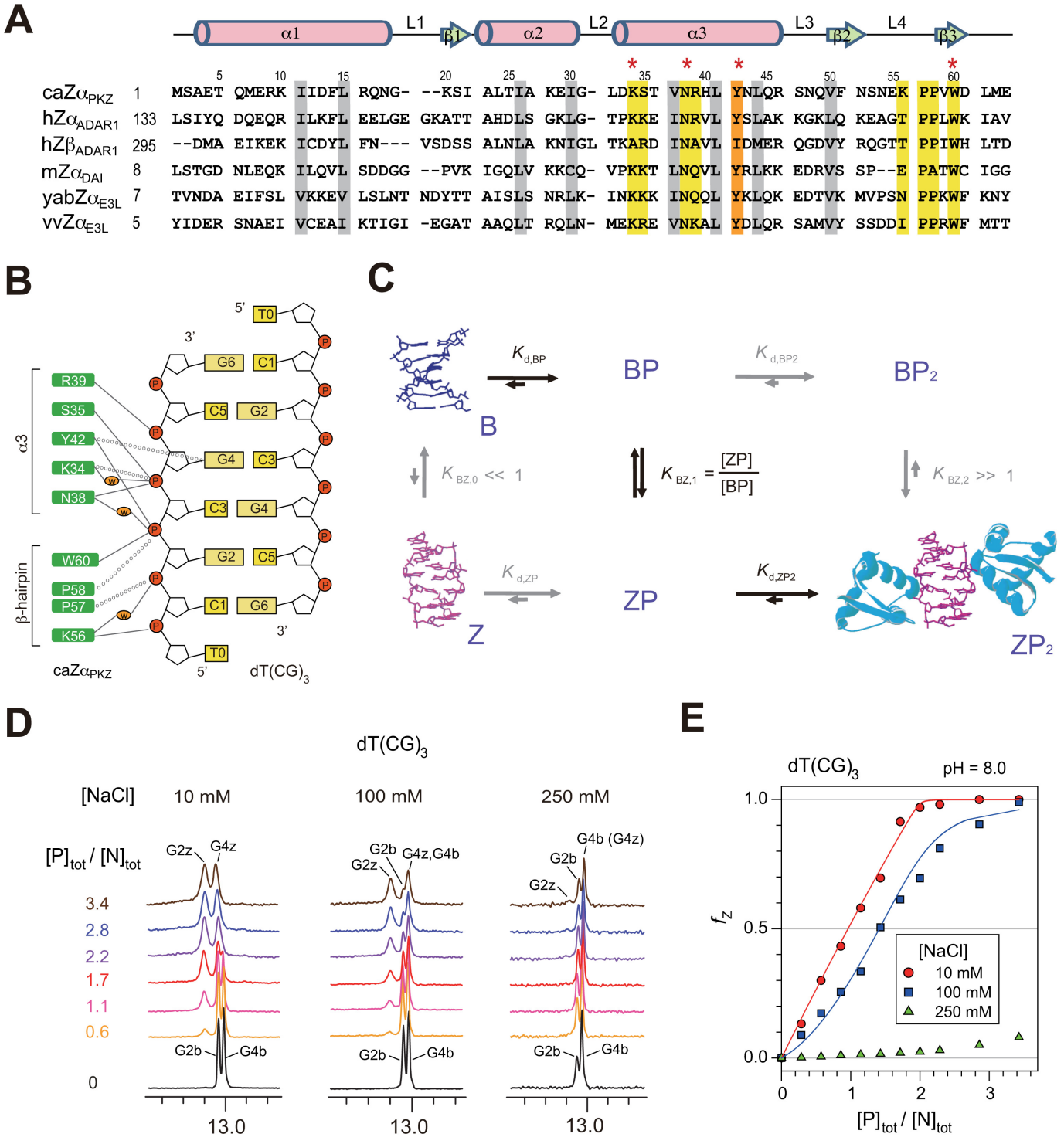

Figure 1. Interaction of caZα$_{PKZ}$ with DNA and its dependence of NaCl concentrations. (**A**) Multiple sequence alignment of Z-DNA binding proteins. Numbering and secondary structural elements for caZα$_{PKZ}$ are shown above the sequence. Yellow and gray bars indicate residues important for Z-DNA recognition and protein folding, respectively. The key aromatic residue, tyrosine, is indicated by an orange bar. The asterisks indicate four highly conserved residues which play important roles in Zα function. (**B**) Residues of caZα$_{PKZ}$ involved in intermolecular interaction with dT(CG)$_3$ reported in a previous study (10). Intermolecular H-bonds and van der Waals contacts indicated by solid lines and dashed lines, respectively. Three water molecules in key positions within the protein–DNA interface are indicated by orange ovals. (**C**) Mechanism for the B–Z conformational transition of a 6-bp DNA by two ZBPs. Black arrows indicate the primary transition mechanism. (**D**) 1D imino proton spectra of dT(CG)$_3$ at 35°C upon titration with caZα$_{PKZ}$ in NMR buffer (pH = 8.0) containing 10 (left), 100 (middle) or 250 mM NaCl (right). The resonances from B-form are labeled as G2b and G4b and those from Z-form are labeled as G2z and G4z. (**E**) Relative Z-DNA populations (f_Z) of dT(CG)$_3$ induced by caZα$_{PKZ}$ at 10 (red circle), 100 (blue square) or 250 mM NaCl (green triangle) as a function of $[P]_{tot}/[N]_{tot}$ ratio. Solid lines are the best fit of the emerging G2z resonance to Equation (8).

Studies of the exchange of imino protons, which reflect the structural and dynamic changes of base-pairs in DNA, have provided the dissociation constants and the equilibrium constant of B–Z transition of a 6-bp DNA induced by hZα$_{ADAR1}$ (11,12) and yabZα$_{E3L}$ (13). However, determination of the DNA-binding sites and conformational changes of ZBPs in each step of the B–Z transition, which relate to their affinities, has not been studied yet. The chemical shift perturbation of ^{15}N-labeled proteins by ligand binding using heteronuclear nuclear magnetic resonance (NMR) has been widely used to identify binding sites as well as to determine binding affinities (14). The NMR titration method has been applied mostly to one-site binding processes but the two-site or more binding systems have rarely been studied quantitatively. Recently, a novel quantitative method to analyze two-site protein interactions by NMR chemical shift perturbation has been described (15). Nevertheless, it is still very difficult to obtain accurate dissociation constants in the DNA–ZBP system, because the ZBPs bind to Z-DNA via a two-site DNA–protein interaction and also induce the B–Z conformational change in the DNA helix (Figure 1C).

In fish species, PKZs contain two Z-DNA binding domains (Zα and Zβ) to recognize heterogeneous DNAs (7,16–18). Although the overall structure of caZα$_{PKZ}$ and its interactions with Z-DNA are very similar to other ZBPs, the B–Z transition activity of caZα$_{PKZ}$ exhibits a unique dependence on NaCl concentration (denoted [NaCl]) (10). In addition, in contrast to other ZBPs, the unusual hydrogen bonding (H-bonding) interaction of caZα$_{PKZ}$-K56 with the phosphate of Z-DNA is required for efficient Z-DNA binding (Figure 1B) (10). Thus the caZα$_{PKZ}$–Z-DNA interaction is thought to be a good model system for the quantitative analysis of a two-site protein–DNA binding system including conformational change of DNA.

In this study, we determined the solution structure of the free form of caZα$_{PKZ}$ by multidimensional heteronuclear NMR spectroscopy and performed NMR experiments on complexes of caZα$_{PKZ}$ with DNA duplexes, dT(CG)$_3$ and d(CG)$_3$, under various [NaCl]. We studied caZα$_{PKZ}$–DNA interactions using imino proton and heteronuclear single-quantum correlation (HSQC) titrations, and determined the dissociation constants of caZα$_{PKZ}$ for B-DNA and Z-DNA binding and the equilibrium constant for the B–Z transition of DNA in the complex form. This provides the information about the chemical shift changes in caZα$_{PKZ}$ upon binding to B-DNA as an intermediate structure during B–Z transition. We also performed relaxation dispersion experiments to kinetically study the Z-DNA binding of caZα$_{PKZ}$. We investigated changes in the binding affinity and hydrogen exchange of d(CG)$_3$ complexed with caZα$_{PKZ}$, in which the H-bonding interaction between Z-DNA and the K56 sidechain of caZα$_{PKZ}$ is interrupted. This study provides structural information on the intermediate complex formed by caZα$_{PKZ}$ and B-DNA, which plays an important role as molecular ruler by deciding the degree to which of the B–Z transition in DNA is induced by ZBPs.

MATERIALS AND METHODS

Sample preparation

The DNA oligomers d(CG)$_3$ and dT(CG)$_3$ were purchased from M-biotech Inc. (the Korean branch of IDT Inc.), purified by reverse-phase HPLC, and desalted using a Sephadex G-25 gel filtration column. The coding sequence for residues 1–75 of caZα$_{PKZ}$ was cloned into *E. coli* expression plasmid pET28a (Novagen, WI, USA). Uniformly ^{13}C/^{15}N- and ^{15}N-labeled caZα$_{PKZ}$ were obtained by growing the transformed BL21(DE3) bacteria cells in M9 medium that contained $^{15}NH_4Cl$ and/or ^{13}C-glucose. The ^{13}C/^{15}N- and ^{15}N-labeled caZα$_{PKZ}$ proteins were purified with a Ni –NTA affinity column and a Sephacryl S-100 gel filtration column (GE Healthcare, USA) on a GE AKTA Prime Plus. The amount of DNA was represented as the concentration of the double-stranded sample. The DNA and protein samples were dissolved in a 90% H_2O/10% D_2O NMR buffer containing 10 mM sodium phosphate (pH = 6.0 or 8.0) and NaCl with concentration of 10, 100 or 250 mM.

NMR experiments

All of the ^{1}H, ^{13}C and ^{15}N NMR experiments were performed on an Agilent DD2 700-MHz spectrometer (GNU, Jinju) or a Bruker Avance-III 800-MHz spectrometer (KBSI, Ochang) equipped with a triple-resonance cryogenic probe. All three-dimensional (3D) triple resonance experiments were carried out with 1.0 mM ^{13}C/^{15}N-labeled caZα$_{PKZ}$ protein. The imino proton and ^{1}H/^{15}N-HSQC spectra were obtained for complexes prepared by addition of ^{15}N-labeled caZα$_{PKZ}$ to 0.1–0.2 mM DNA or addition of DNA to 1 mM ^{15}N-labeled caZα$_{PKZ}$. One dimensional (1D) NMR data were processed with either VNMR J (Agilent, Santa Clara, CA, USA) or FELIX2004 (FELIX NMR, San Diego, CA, USA) software, while the two-dimensional and 3D data were processed with NMRPIPE (19) and analyzed with Sparky (20). External 2–2-dimethyl-2-silapentane-5-sulfonate was used for the ^{1}H, ^{13}C and ^{15}N references.

^{1}H, ^{13}C and ^{15}N resonance assignments for caZα$_{PKZ}$ were obtained from the following 3D experiments in 10% D_2O/90% H_2O containing 10 mM sodium phosphate (pH 8.0) and 100 mM NaCl: CACB(CO)NH, HNCA, HNCACB, HNCO, HAHB(CO)NH, CB(CGCD)HD, CB(CGCCDCE)HE, HCCH-TOCSY, NOESY-^{1}H/^{15}C-HSQC, NOESY-^{1}H/^{15}N-HSQC and TOCSY-^{1}H/^{15}N-HSQC. The average chemical shift differences of the amide proton and nitrogen resonances between the two states were calculated by Equation (1):

$$\Delta\delta_{avg} = \sqrt{(\Delta\delta_H)^2 + (\Delta\delta_N/5.88)^2} \quad (1)$$

where $\Delta\delta_H$ and $\Delta\delta_N$ are the chemical shift differences of the amide proton and nitrogen resonances, respectively.

Solution structure calculation

The inter-proton distance restraints were extracted from NOESY-^{1}H/^{15}N-HSQC and NOESY-^{1}H/^{13}C-HSQC spectra. Backbone dihedral angle restraints were generated using TALOS+ (21). Only phi (φ) and psi (ψ) angle restraints

which qualified as 'good' predictions from TALOS+ were used in the structure calculation. Hydrogen-bonds were introduced as a pair of distance restraints based on nuclear Overhauser effect (NOE) analysis in combination with the prediction of protein secondary structural elements using the software CSI (22). Structure calculations were initially performed with CYANA 2.1, which combines automated assignment of NOE cross-peaks and structure calculation. On the basis of distance restraints derived from CYANA output, further structure calculations were carried out using CNS 1.3 in explicit solvent using the RECOORD protocol (23–25). The 10 lowest-energy structures were validated by PROCHECK-NMR (26). Structures were visualized using the program Discovery Studio 4.1 (BIOVIA, San Diego, CA, USA). Structural statistics are presented in Table 1.

Nitrogen Carr-Purcell-Meiboom-Gill (CPMG) relaxation dispersion

The ^{15}N amide Carr-Purcell-Meiboom-Gill (CPMG) relaxation dispersion experiments were performed using free ^{15}N-labeled caZα$_{PKZ}$ and ^{15}N-labeled caZα$_{PKZ}$ complexed with dT(CG)$_3$ at 35°C. Experiments employed a constant relaxation delay (T_{relax}) of 60 ms and 11 values of $\nu_{CPMG} = 1/(2\tau_{CP})$ ranging from 33 to 900 Hz, τ_{CP} is the delay between consecutive pulses. Transverse relaxation rates $R_{2,eff}$ were calculated for each cross-peak signal at each value by:

$$R_{2,\mathrm{eff}}(\nu_{\mathrm{CPMG}}) = -\frac{1}{T_{\mathrm{relax}}} \ln\left(\frac{I(\nu_{\mathbf{CPMG}})}{I_0}\right) \quad (2)$$

where $I(\nu_{CPMG})$ and I_0 are the peak intensity at values of ν_{CPMG} with of 60 and 0 ms, respectively. For evaluation of average and standard deviation of $R_{2,eff}$ values, three or four different datasets were measured.

In the free caZα$_{PKZ}$, the relaxation dispersions derived from residues in fast exchange on the NMR chemical shift timescale were fitted to (27):

$$R_{2,\mathrm{eff}}^{\mathrm{free}}(\nu_{\mathrm{CPMG}}) = R_2^0 + \frac{\Phi_{\mathrm{ex,f}}}{k_{\mathrm{ex,f}}}\left\{1 - \frac{4\nu_{\mathrm{CPMG}}}{k_{\mathrm{ex,f}}}\tanh\left(\frac{k_{\mathrm{ex,f}}}{4\nu_{\mathrm{CPMG}}}\right)\right\} \quad (3)$$

where $R^0{}_2$ is the intrinsic transverse relaxation rate; $\Phi_{ex,f} = p_A p_B(\Delta\omega_f)^2$, where $\Delta\omega_f$ is chemical shift difference between states A and B and p_A and p_B are the relative populations of states A and B, respectively; and $k_{ex,f}$ the exchange rate between states A and B. The caZα$_{PKZ}$ in the complex with Z-DNA shows two kinds of independent exchange processes, the conformational exchange of free protein and the association/dissociation of Z-DNA. In this case, the relaxation dispersion data of the caZα$_{PKZ}$ complexed with dT(CG)$_3$ ($R_{2,eff}{}^{comp}$) could be expressed by Equation (4):

$$R_{2,\mathrm{eff}}^{\mathrm{comp}}(\nu_{\mathrm{CPMG}}) = R_2^0 + R_{2,\mathrm{eff}}^{\mathrm{free}}(\nu_{\mathrm{CPMG}}) + \frac{\Phi_{\mathrm{ex,b}}}{k_{\mathrm{ex,b}}}\left\{1 - \frac{4\nu_{\mathrm{CPMG}}}{k_{\mathrm{ex,b}}}\tanh\left(\frac{k_{\mathrm{ex,b}}}{4\nu_{\mathrm{CPMG}}}\right)\right\} \quad (4)$$

where $R^0{}_2$ is the intrinsic transverse relaxation rate; $\Phi_{ex,b} = p_b p_u(\Delta\omega_{bound})^2$, where $\Delta\omega_{bound}$ is chemical shift difference between the bound and unbound states and p_b and p_u are the relative populations of the bound and unbound states, respectively; and $k_{ex,b}$ the exchange rate between the bound and unbound states (28).

Binding models

Accordingly, the HSQC titration curves were analyzed by assuming an *active* model of B–Z transition (Figure 1C), where **P** is the free forms of caZα$_{PKZ}$, **BP** and **ZP** are the singly bound forms to B-DNA and Z-DNA, respectively, **ZP$_2$** is the doubly bound form to Z-DNA, and **B** is the B-form of free dT(CG)$_3$. The concentrations of **B**, **BP**, **ZP** and **ZP$_2$** forms, [B], [BP], [ZP] and [ZP$_2$], respectively, are described as:

$$[\mathrm{B}] = [N]_{\mathrm{tot}}\frac{K_{\mathrm{d,BP}}K_{\mathrm{d,ZP2}}}{K_{\mathrm{d,BP}}K_{\mathrm{d,ZP2}} + (1+K_{\mathrm{BZ,1}})K_{\mathrm{d,ZP2}}[P] + K_{\mathrm{BZ,1}}[P]^2}$$

$$[\mathrm{BP}] = [N]_{\mathrm{tot}}\frac{K_{\mathrm{d,ZP2}}[P]}{K_{\mathrm{d,BP}}K_{\mathrm{d,ZP2}} + (1+K_{\mathrm{BZ,1}})K_{\mathrm{d,ZP2}}[P] + K_{\mathrm{BZ,1}}[P]^2}$$

$$[\mathrm{ZP}] = [N]_{\mathrm{tot}}\frac{K_{\mathrm{BZ,1}}K_{\mathrm{d,ZP2}}[P]}{K_{\mathrm{d,BP}}K_{\mathrm{d,ZP2}} + (1+K_{\mathrm{BZ,1}})K_{\mathrm{d,ZP2}}[P] + K_{\mathrm{BZ,1}}[P]^2}$$

$$[\mathrm{ZP_2}] = [N]_{\mathrm{tot}}\frac{K_{\mathrm{BZ,1}}[P]^2}{K_{\mathrm{d,BP}}K_{\mathrm{d,ZP2}} + (1+K_{\mathrm{BZ,1}})K_{\mathrm{d,ZP2}}[P] + K_{\mathrm{BZ,1}}[P]^2} \quad (5)$$

where $[N]_{tot}$ is the total concentration of DNA duplex; $K_{d,BP}$ and $K_{d,ZP2}$ are the dissociation constants for the **BP** and **ZP$_2$** complexes, respectively; $K_{BZ,1}$ (= [ZP]/[BP]) is the equilibrium constant between **BP** and **ZP** forms; and $[P]$ is the concentration of the free caZα$_{PKZ}$, which is a solution of the following cubic equation:

$$[P]^3 + a[P]^2 + b[P] + c = 0 \quad (6)$$

$$a = 2[N]_{\mathrm{tot}} - [P]_{\mathrm{tot}} + \left(1 + \frac{1}{K_{\mathrm{BZ,1}}}\right)K_{\mathrm{d,ZP2}}$$

$$b = \left(1 + \frac{1}{K_{\mathrm{BZ,1}}}\right)K_{\mathrm{d,ZP2}}([N]_{\mathrm{tot}} - [P]_{\mathrm{tot}}) + \frac{K_{\mathrm{d,BP}}K_{\mathrm{d,ZP2}}}{K_{\mathrm{BZ,1}}}$$

$$c = -\frac{K_{\mathrm{d,BP}}K_{\mathrm{d,ZP2}}}{K_{\mathrm{BZ,1}}}[P]_{\mathrm{tot}}$$

where $[P]_{tot}$ is the total concentration of caZα$_{PKZ}$. The closed-form solution of Equation (6) has been reported (29):

$$[P] = -\frac{a}{3} + \frac{2}{3}\sqrt{a^2 - 3b}\cos\frac{\theta}{3} \quad (7)$$

where,

$$\theta = \arccos\frac{-2a^3 + 9ab - 27c}{2\sqrt{(a^2 - 3b)^3}}$$

The observed ^{1}H and ^{15}N chemical shift difference referenced to the free caZα$_{PKZ}$, $\Delta\delta_{obs}$, is described as:

$$\Delta\delta_{\mathrm{obs}} = \frac{[\mathrm{BP}]}{[P]_{\mathrm{tot}}}\Delta\delta_{\mathrm{B}} + \frac{[\mathrm{ZP}] + 2[\mathrm{ZP_2}]}{[P]_{\mathrm{tot}}}\Delta\delta_{\mathrm{Z}} \quad (8)$$

Table 1. Structural statistics for the caZα$_{PKZ}$ structures

NOE upper distance limits	878
Intra-residual	241
Short-range (|i – j| = 1)	312
Medium-range (1 < | i – j | < 5)	210
Long-range (|i – j | > = 5)	63
Dihedral angle constraints	109
Hydrogen bonds	27 × 2
Violations	
Distances > 0.5 Å	none
Dihedral angles > 5°	none
Ramachandran analysis (%)	
Most favored regions	79.3
Additionally allowed regions	15.5
Generously allowed regions	5.2
Disallowed regions	0.0
R.M.S.D. from mean structure (structured region)[a]	
Backbone (Å)	0.57 ± 0.18
Heavy atom (Å)	1.04 ± 0.21

[a]Residues in the structured region: 6–61.

where $\Delta\delta_B$ and $\Delta\delta_Z$ are the ^{1}H and ^{15}N chemical shift differences of the B-DNA- and Z-DNA-bound forms relative to the free form, respectively. The relative Z-DNA population (f_Z) could be determined from the integration of new resonances in the ^{31}P NMR or imino proton spectra, which provide the same results (11). The observed f_Z value determined from imino proton resonances is described as:

$$f_Z = \frac{[ZP] + [ZP_2]}{[N]_{tot}} \quad (9)$$

Hydrogen exchange rate measurement

The apparent longitudinal relaxation rate constants ($R_{1a} = 1/T_{1a}$) of the imino protons of free and bound DNA were determined by semi-selective inversion recovery 1D NMR experiments. The hydrogen exchange rate constants (k_{ex}) of the imino protons were measured by a water magnetization transfer experiment with 20 different delay times (30,31). The k_{ex} values for the imino protons were determined by fitting the data to Equation (10):

$$\frac{I_0 - I(t)}{I_0} = 2\frac{k_{ex}}{(R_{1w} - R_{1a})}\left(e^{-R_{1a}t} - e^{-R_{1w}t}\right) \quad (10)$$

where I_0 and $I(t)$ are the peak intensities of the imino proton at times zero and t, respectively, and R_{1a} and R_{1w} are the apparent longitudinal relaxation rate constants for the imino proton and water, respectively (30–32).

RESULTS

Titration of caZα$_{PKZ}$ into dT(CG)$_3$ under various [NaCl]

Figure 1D shows the changes in the imino-proton spectra of dT(CG)$_3$ upon titration with caZα$_{PKZ}$ at 35°C. The relative populations of Z-DNA (f_Z) in dT(CG)$_3$ were determined by integration of the new G2z resonance, as a function of the total protein: total DNA duplex ($[P]_{tot}/[N]_{tot}$) ratio (Figure 1E). CaZα$_{PKZ}$ exhibited a severe decrement in B–Z transition activity as [NaCl] increased. Most of the dT(CG)$_3$ was in the Z-conformation at $[P]_{tot}/[N]_{tot}$ > 2.0 at 10 mM NaCl. However, at [NaCl] = 100 mM, only about 67% of dT(CG)$_3$ displayed the Z-DNA conformation at $[P]_{tot}/[N]_{tot} = 2.0$ (Figure 1E), in contrast to previous findings that most of d(CG)$_3$ was converted to Z-DNA by hZα$_{ADAR1}$ (11) and yabZα$_{E3L}$ (13) under the same conditions. Interestingly, when [NaCl] increased up to 250 mM, caZα$_{PKZ}$ showed extremely low B–Z transition activity to dT(CG)$_3$ (Figure 1E).

Solution structure of free caZα$_{PKZ}$

In order to elucidate detailed structural information for free caZα$_{PKZ}$, the solution structure of free caZα$_{PKZ}$ was determined by restrained molecular dynamics calculations using 878 distance restraints and 109 dihedral angle restraints collected at 100 mM NaCl (Table 1). A final set of 10 lowest energy structures was selected from 100 calculations, with no violations larger than 0.5 Å and 5° for the NOEs and dihedral angles, respectively (Figure 2A). The RMSD values for the backbone atoms in structured region was calculated to be 0.57 ± 0.18 Å. Free caZα$_{PKZ}$ is composed of three α-helices (α1, α2 and α3) and three β-strands (β1, β2 and β3) (Figure 2A). The ensemble of the 10 lowest energy structures shows that only the L4 loop in the β-hairpin (residues 53–57) is not well converged whereas all other loops are tightly structured (Figure 2A). Two consecutive prolines (P57 and P58) which have only limited numbers of restraints hinder to determine the precise orientation of the β-hairpin in solution structures. Figure 2B shows the superimposition of the lowest energy structure of free caZα$_{PKZ}$ and the crystal structure of the caZα$_{PKZ}$–dT(CG)$_3$ complex (10), where the β-hairpin exhibits bigger differences while no significant structural deviations were observed in other structural regions. The crystal structure showed that K56 sidechain in the β-hairpin of caZα$_{PKZ}$ is involved in H-bonding with the phosphate of Z-DNA in the caZα$_{PKZ}$–dT(CG)$_3$ complex (10) (Figure 2B). It might be possible that the orientation of the β-hairpin is restrained when the sidechain of K56 interacts with the backbone of Z-DNA.

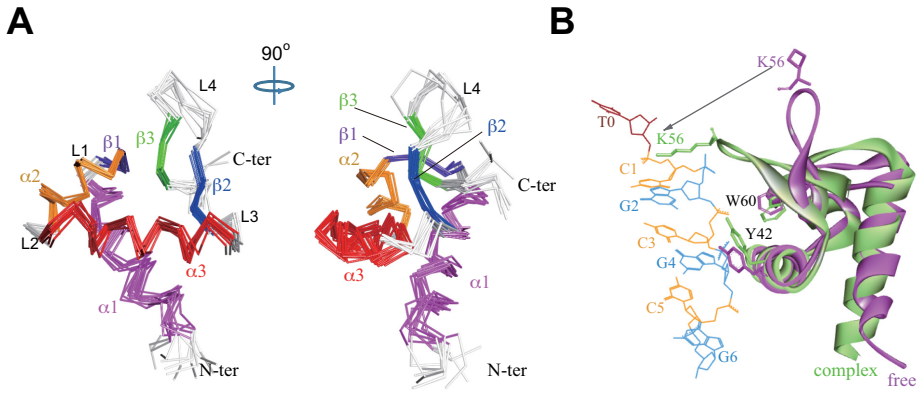

Figure 2. Solution structure of free caZα$_{PKZ}$ and comparison with other structures. (**A**) Superimposed backbone traces of the 10 lowest energy caZα$_{PKZ}$ structures. (**B**) Superimposition of the 3D structures of free caZα$_{PKZ}$ (violet) and caZα$_{PKZ}$–dT(CG)$_3$ complex (PDB ID = 4KMF, pale green).

Chemical shift changes in caZα$_{PKZ}$ upon binding to dT(CG)$_3$

In the ^{1}H/^{15}N-HSQC spectra of free caZα$_{PKZ}$ and caZα$_{PKZ}$–dT(CG)$_3$ at 35°C, the amide resonances for several residues (N38, R39 and Y42) of the α3 helix disappeared altogether (Supplementary Figure S2), meaning they were in chemical exchange on an intermediate NMR time scale. Significant chemical shift changes were observed in other residues in the α3 helix as well as most residues in the β1–α2 and β-hairpin regions (Supplementary Figure S1), indicating the direct interaction of the sidechains of caZα$_{PKZ}$ with the phosphate backbone of dT(CG)$_3$ as reported in the previous crystal structural study (10). As expected from the imino proton spectra at 250 mM NaCl, few chemical shift changes occurred upon exposure to dT(CG)$_3$ (Supplementary Figure S1).

To further clarify the chemical shift perturbation results, the ^{1}H/^{15}N-HSQC spectra of caZα$_{PKZ}$ were acquired at 35°C as a function of the $[N]_{tot}/[P]_{tot}$ ratio, where most amide cross-peaks showed significant movement (Supplementary Figure S2). Interestingly, the cross-peaks of some residues changed the direction of their movement after achieving a certain position (Figure 3A and Supplementary Figure S2), indicating the presence of at least two binding modes. We analyzed the HSQC titration curves as well as the relative Z-DNA populations (f_Z) assuming an *active* B–Z transition model (Figure 1C). $K_{d,BP}$ and $K_{d,ZP2}$ are the dissociation constants of the **BP** and **ZP$_2$** complexes, respectively, and $K_{BZ,1}$ (= [ZP]/[BP]) is the equilibrium constant between the **ZP** and **BP** complexes. Because fitting each titration curve independently did not give reliable K_d values, all titration curves were fitted globally. During global fitting, we have fitted simultaneously all ^{1}H and ^{15}N titration curves with Equation (8) and the f_Z data with Equation (9) to obtain accurate K_d values (Figure 3B–D). At 10 mM NaCl, the global fitting gave $K_{d,BP}$ and $K_{d,ZP2}$ of 28 ± 17 and 345 ± 79 nM, respectively, and $K_{BZ,1}$ of 0.87 ± 0.01 (Table 2 and Figure 3B and C). The dataset at 100 mM NaCl was globally fitted to obtain $K_{d,BP}$ and $K_{d,ZP2}$ values of 16.4 ± 0.8 and 8.76 ± 0.67 μM, respectively, and $K_{BZ,1}$ of 0.19 ± 0.01 (Table 2 and Figure 3B and D). These results indicate that the incrementation of [NaCl] from 10 to 100 mM leads to ∼600- and 25-fold larger K_d of caZα$_{PKZ}$ for B-DNA and Z-DNA binding, respectively, and 4.6-fold lower B–Z transition activity in the complex form (Table 2). The titration data at 250 mM NaCl could not be analyzed based on an *active* B–Z transition model, because of the extremely smaller $K_{BZ,1}$.

Chemical shift differences in caZα$_{PKZ}$ bound to B-DNA and Z-DNA

In addition to the dissociation constants, the global fitting method also provides the ^{1}H and ^{15}N chemical shift differences between the free and the bound forms for both B-DNA and Z-DNA binding (Supplementary Figure S3). The combined averages of ^{1}H and ^{15}N chemical shift changes ($\Delta\delta_{avg}$) were determined for each residue to represent effects of binding to B-DNA and Z-DNA (Figure 4A). The chemical shift information for residues N38, R39, L41, Y42 and L44 in the α3 helix could not be collected because these resonances disappeared or became very weak during titration upon DNA. At 10 mM NaCl, both B-DNA and Z-DNA binding of caZα$_{PKZ}$ caused similar chemical shift perturbations, such that significant chemical shift changes were observed in the α3 helix as well as in the β1–α2 and β-hairpin regions (Figure 4A). However, at 100 mM NaCl, the B-DNA and Z-DNA binding of caZα$_{PKZ}$ exhibited completely different chemical shift perturbation results from each other (Figure 4A). For the Z-DNA binding, a large chemical shift changes were observed for the α3, β1–α2 and β-hairpin regions, similar to data at 10 mM NaCl (Figure 4A and B). On the other hand, the B-DNA binding affected I30 in L2; S35, Q45 and R46 in α3; and N54 and V59 in the β-hairpin with $\Delta\delta_{avg} > 0.06$ ppm (Figure 4A and C). These results meant that the B-DNA binding state of caZα$_{PKZ}$ exhibited distinct structural features under high and low salt conditions, which might be related to reduced B–Z transition activity at higher [NaCl].

The superimposed ^{1}H/^{15}N-HSQC spectra of free caZα$_{PKZ}$ at 10, 100 or 250 mM NaCl at 25°C are shown in Supplementary Figure S4. Significant chemical shift differences were observed for residues in the α2 and α3 regions with increasing [NaCl] from 10 to 100 mM (Figure 4D). However, all residues in the Z-DNA binding complex showed little chemical shift changes ($\Delta\delta_{avg} < 0.05$ ppm)

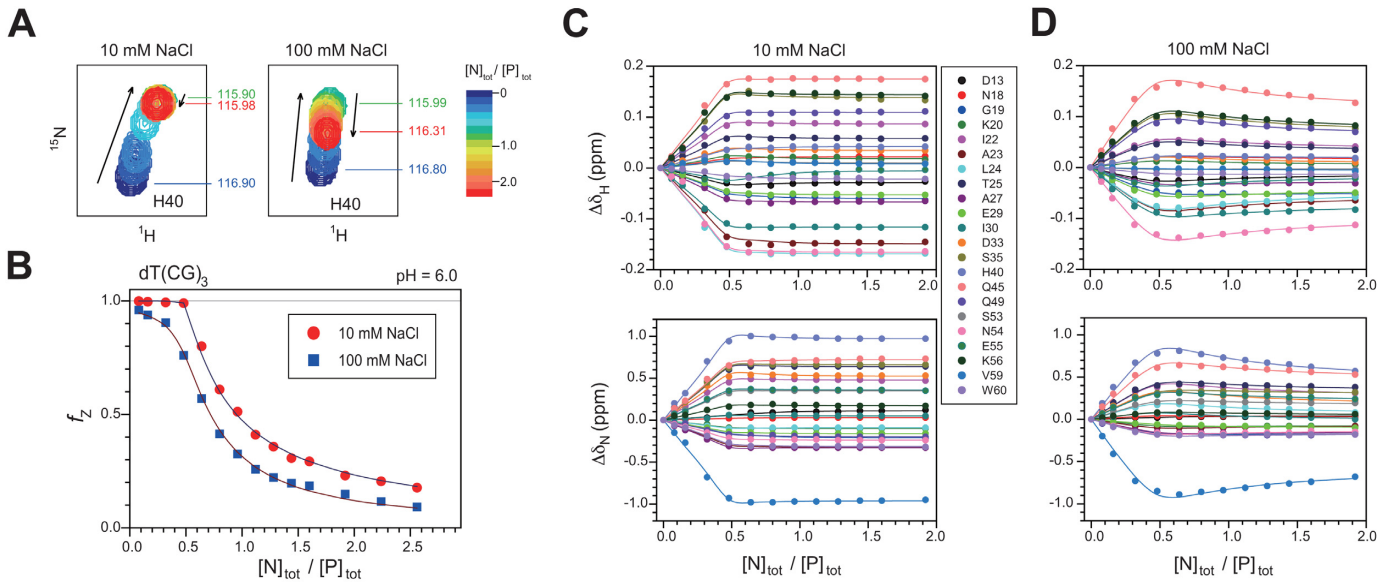

Figure 3. Quantitative assessments of DNA binding by caZα$_{PKZ}$ using HSQC data. (**A**) A representative region of the $^{1}H/^{15}N$-HSQC of caZα$_{PKZ}$ upon titration with dT(CG)$_3$ at 10 (left) or 100 mM NaCl (right). The cross-peak color changes gradually from blue (free) to red (bound) according to the $[N]_{tot}/[P]_{tot}$ ratio. (**B**) Global fitting of the f_Z data and (**C** and **D**) the $^{1}H/^{15}N$-HSQC titration curves for caZα$_{PKZ}$ with dT(CG)$_3$ as a function of $[N]_{tot}/[P]_{tot}$ ratio. Data for the global fitting were derived from ^{1}H (upper) and ^{15}N (lower) chemical shift changes of HSQC cross-peaks of caZα$_{PKZ}$ at (C) 10 or (D) 100 mM NaCl. Solid lines are the best fits to Equation (8) (in B) or Equation (7) (in C and D).

Table 2. Dissociation constants ($K_{d,BP}$ and $K_{d,ZP2}$) for B-DNA and Z-DNA binding, equilibrium constant for B–Z transition ($K_{BZ,1}$) and association/dissociation rate constants ($k_{on,ZP}$ and $k_{off,ZP2}$) for Z-DNA binding of caZα$_{PKZ}$ with a 6-bp DNA

DNA	pH	[NaCl] (mM)	$K_{d,BP}$ (μM)	$K_{d,ZP2}$ (μM)	$K_{BZ,1}$	$k_{on,ZP}$ ($\times 10^8$ $M^{-1}s^{-1}$)	$k_{off,ZP2}$ (s^{-1})
dT(GC)$_3$	6.0	10	0.028 ± 0.017	0.345 ± 0.079	0.87 ± 0.03	19.6 ± 1.2[a]	675 ± 43[a]
		100	16.4 ± 0.8	8.76 ± 0.67	0.19 ± 0.02	1.56 ± 0.03[b]	1381 ± 30[b]
	8.0	10	0.157 ± 0.021	0.129 ± 0.074	1.18 ± 0.03		
		100	5.41 ± 0.66	2.41 ± 0.37	0.18 ± 0.02		
d(GC)$_3$	8.0	10	5.18 ± 2.43	1.79 ± 0.95	0.11 ± 0.05		

[a]From CPMG data with $P_{free} = 0.873$.
[b]From CPMG data with $P_{free} = 0.891$.

upon change of [NaCl] (Figure 4D). For example, the A23 and L24 amide signals in the Z-DNA binding complex were located at the almost same position in the spectra (red and orange peaks in Figure 4E), whereas they showed the significant chemical shift differences in the free form (green and brown peaks in Figure 4E). These results indicate that the Z-DNA binding complex of caZα$_{PKZ}$ maintains almost the same structural features regardless of salt concentration, contrary to free caZα$_{PKZ}$.

^{15}N Carr-Purcell-Meiboom-Gill (CPMG) relaxation dispersion experiment on caZα$_{PKZ}$ bound to dT(CG)$_3$

The rate constants for association and dissociation of caZα$_{PKZ}$ with DNA were determined using NMR ^{15}N backbone amide CPMG relaxation dispersion experiments (33). According to the concentrations of each state calculated using Equation (4) as a function of $[N]_{tot}/[P]_{tot}$, free **P** and complex **ZP$_2$** are the only two major conformational states when $[N]_{tot}/[P]_{tot} << 0.5$ (Supplementary Figure S5). Thus we analyzed the CPMG data using a two-state model of conformational exchange, where the **ZP** and **ZP$_2$** are considered as the ligand (L) and complex (PL), respectively (Figure 5A). In this model, the conformation exchange rate (k_{ex}) is given by $k_{ex} = k_{on,ZP}[ZP] + k_{off,ZP2}$, where $k_{on,ZP}$ is the association rate of **ZP**, $k_{off,ZP2}$ is the dissociation rate of **ZP$_2$** and [ZP] is the concentration of **ZP** (Figure 5A). Interestingly, several residues of free caZα$_{PKZ}$ exhibited conformational exchange with k_{ex} of 550 ± 296 and 684 ± 153 s^{-1} at 10 and 100 mM NaCl, respectively (Figure 5B). Thus, in order to minimize the effect of conformational exchange of free caZα$_{PKZ}$, the transverse relaxation rate differences between the caZα$_{PKZ}$–dT(CG)$_3$ complex and free caZα$_{PKZ}$ ($R_{2,eff}^{comp} - R_{2,eff}^{free}$) were fitted globally using Equation (4). The Δω values were determined from global fitting of the $^{1}H/^{15}N$ titration data and the relative population of free caZα$_{PKZ}$, p_{free} ($= [P]/[P]_{tot}$) was calculated by $p_{free} = 1 - \Delta\delta_{obs}/\Delta\delta_Z$ (Figure 5C). Even though we used these fixed Δω and p_{free} values for fitting of the CPMG data, the all CPMG data were globally well fitted (Figure 5D). It indicates that the conformation exchange for the association/dissociation of Z-DNA exhibits the single k_{ex} value through all residues. At 10 mM NaCl, the CPMG

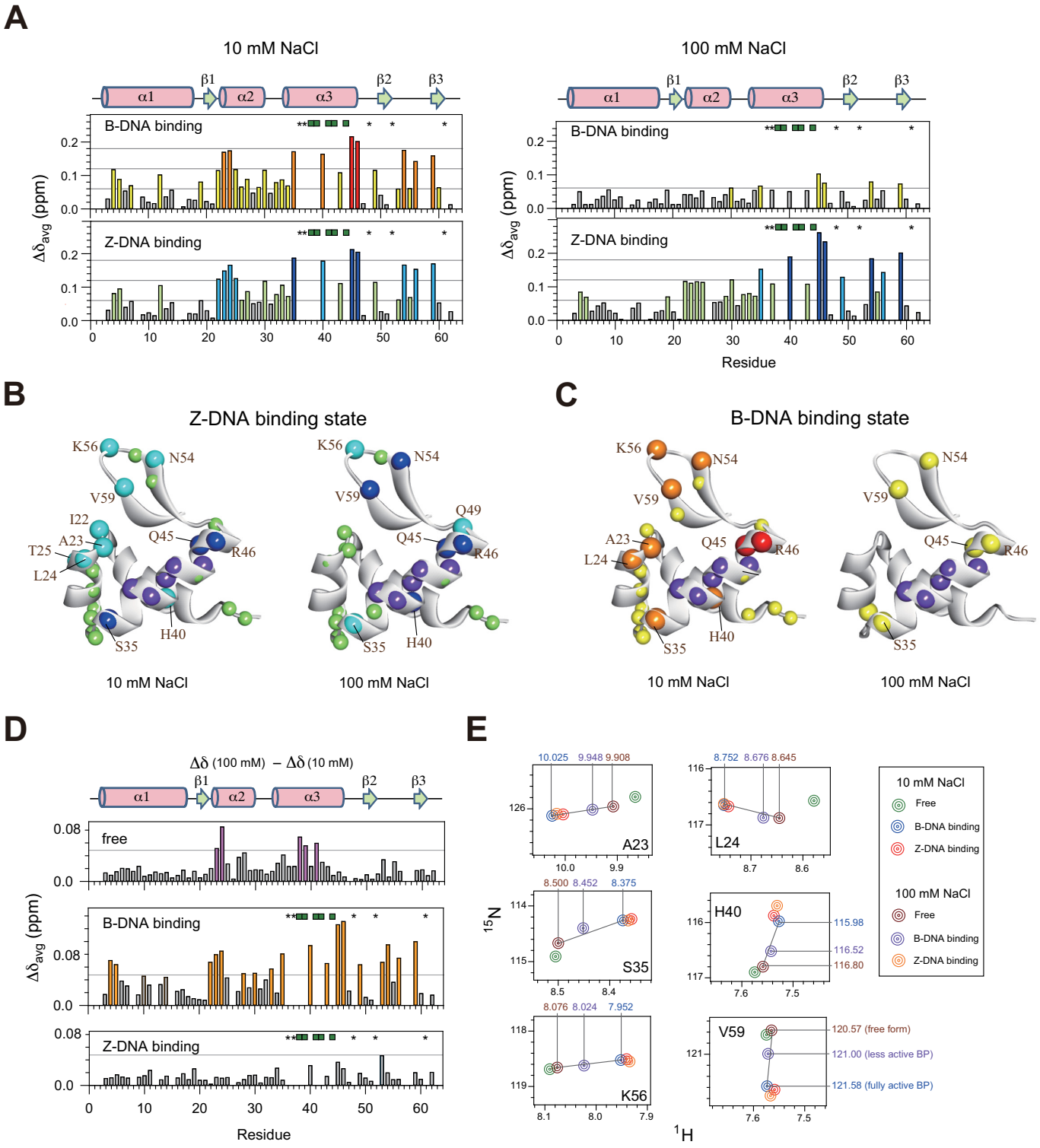

Figure 4. DNA binding patterns differ with salt concentration and DNA conformation. (**A**) Histograms of the $\Delta\delta_{avg}$ values of ^{15}N-ca$Z\alpha_{PKZ}$ for the B-DNA and Z-DNA binding at 10 (left) or 100 mM NaCl (right). Residues whose cross-peaks disappear or become very weak during titration are represented with green square symbols. The asterisks indicate residues whose cross-peaks overlap with other resonances during titration. (**B** and **C**) Mapping the location of the residues having large $\Delta\delta_{avg}$ onto the NMR structure of free ca$Z\alpha_{PKZ}$ for the (B) Z-DNA and (C) B-DNA binding at 10 (left) or 100 mM NaCl (right). The colors used to illustrate the $\Delta\delta_{avg}$ are: red or blue, >0.18 ppm; orange or cyan, 0.12–0.18 ppm; and yellow or pale green, 0.08–0.12 ppm (the same color coding is used in panel A). In both panels, the purple spheres indicate residues whose cross-peaks disappear or become very weak during titration. (**D**) The average chemical shift differences ($\Delta\delta_{avg}$) between [NaCl] of 10 and 100 mM for free ca$Z\alpha_{PKZ}$ (upper) and ca$Z\alpha_{PKZ}$ complexed with B-DNA (middle) and Z-DNA (lower). (**E**) The calculated ^{1}H/^{15}N-HSQC cross-peaks of ca$Z\alpha_{PKZ}$ complexed with B-DNA and Z-DNA in buffer containing 10 or 100 mM NaCl.

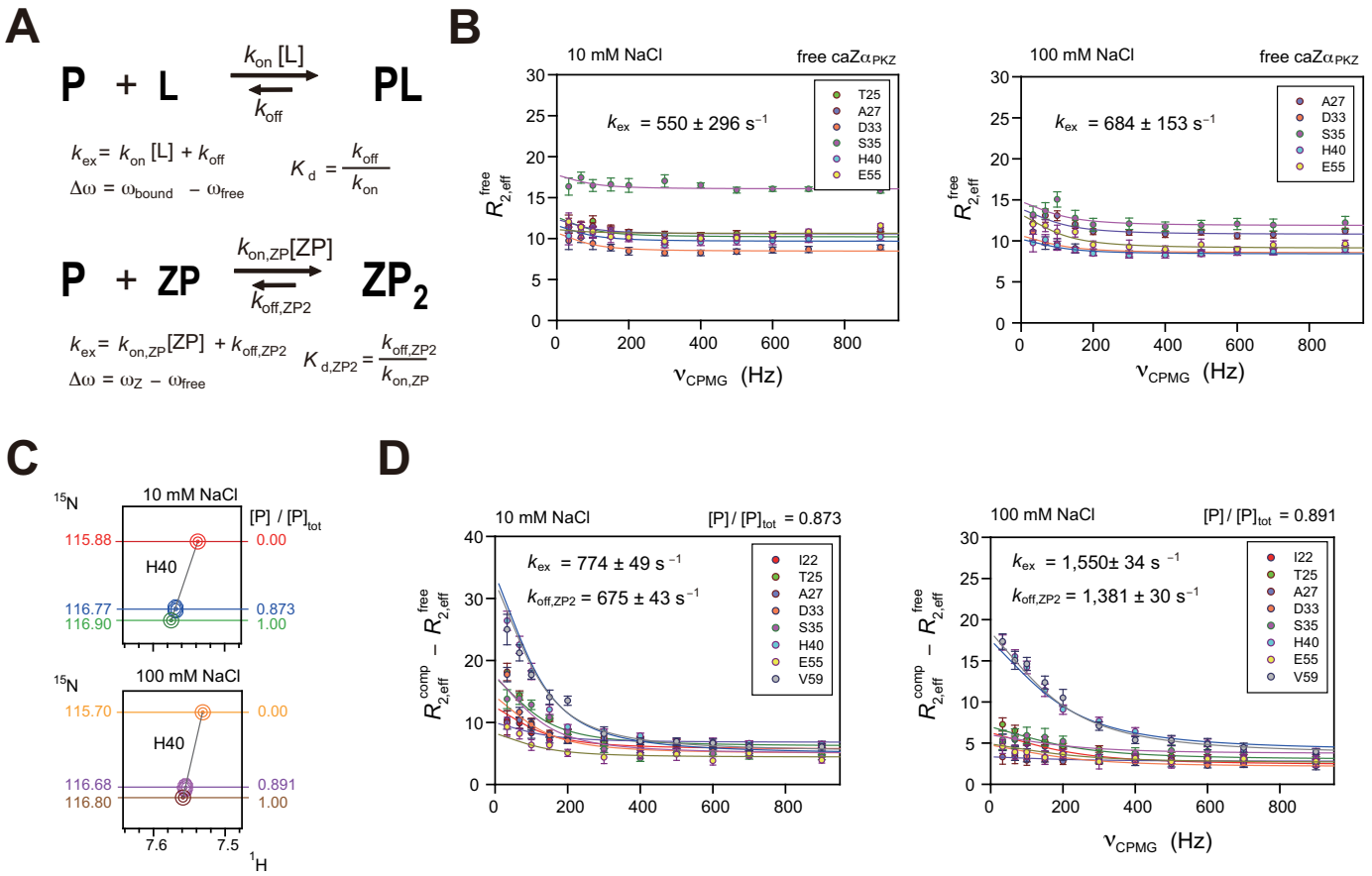

Figure 5. Quantitative assessments of DNA binding by caZα$_{PKZ}$ using CPMG data. (**A**) Two-state models of association/dissociation of a protein–ligand complex (upper) and the caZα$_{PKZ}$–Z-DNA complex (lower). (**B**) The ^{15}N CPMG NMR relaxation dispersion data for free caZα$_{PKZ}$ with [NaCl] of 10 (left) or 100 mM (right). (**C**) The simulated ^{1}H/^{15}N-HSQC cross-peaks of H40 of the caZα$_{PKZ}$–dT(CG)$_3$ complex at 10 (upper) or 100 mM NaCl (lower). The ^{15}N chemical shifts and calculated $[P]/[P]_{tot}$ ratio are shown left and right of the spectra, respectively. (**D**) The ^{15}N CPMG NMR relaxation dispersion data for the caZα$_{PKZ}$–dT(CG)$_3$ complex at 10 (left) or 100 mM NaCl (right). The microscopic rate constant ($k_{off,ZP2}$) was extracted from k_{ex} and the $[P]/[P]_{tot}$ ratio.

dataset with $p_{free} = 0.873$ was globally fit to obtain the k_{ex} of 774 ± 49 s^{-1}, which was used to calculate the $k_{on,ZP}$[ZP] and $k_{off,ZP2}$ of 98 ± 6 and 675 ± 43 s^{-1}, respectively (using $k_{off,ZP2} = k_{ex} \times p_{free}$) and the $k_{on,ZP}$ of (1.96 ± 0.12) × 10^9 M^{-1}s^{-1} (using $k_{on,ZP} = k_{off,ZP2}/K_{d,ZP2}$) (Table 2 and Figure 5D). In the case that [NaCl] = 100 mM, the dataset at p_{free} = 0.891 was globally fitted to obtain the k_{ex} of 1550 ± 34 s^{-1} and the $k_{off,ZP2}$ and $k_{on,ZP}$ of 1381 ± 30 and (1.56 ± 0.03) × 10^8 M^{-1}s^{-1}, respectively (Table 2 and Figure 5D). These results indicate that, as [NaCl] increased from 10 to 100 mM, the 13-fold slower $k_{on,ZP}$ and 2-fold faster $k_{off,ZP2}$ resulted in a 25-fold larger $K_{d,ZP2}$.

H-bonding interaction of K56 with Z-DNA phosphate

The crystal structure of the caZα$_{PKZ}$–dT(CG)$_3$ complex showed that the sidechain of K56 exhibited an unusual H-bonding interaction with the T0pC1 phosphate of Z-DNA (Figure 1B) (10). Thus, in order to understand the role of this intermolecular H-bonding interaction, NMR titrations of caZα$_{PKZ}$ into d(CG)$_3$ were performed (Figure 6A). At 10 mM NaCl, only 57% of d(CG)$_3$ was converted to Z-DNA by caZα$_{PKZ}$ at $[P]_{tot}/[N]_{tot} = 2.0$ (Figure 6B), whereas most of dT(CG)$_3$ exhibited the Z-DNA conformation at $[P]_{tot}/[N]_{tot} \geq 2.0$ (Figure 1E). A similar decrement in B–Z transition activity was also observed at 100 mM NaCl (Figure 6B). We fitted simultaneously the ^{1}H and ^{15}N titration curves of caZα$_{PKZ}$ and the f_Z data of d(CG)$_3$ and dT(CG)$_3$ at pH 8.0 to compare the B–Z transition activities of these two DNAs by caZα$_{PKZ}$ (Supplementary Figure S6). The global fitting showed that d(CG)$_3$ has 33- and 14-fold larger values of $K_{d,BP}$ and $K_{d,ZP2}$, respectively, and a 10-fold smaller $K_{BZ,1}$ than dT(CG)$_3$ at 10 mM NaCl (Table 2). When [NaCl] = 100 mM, the ^{1}H/^{15}N-HSQC titration data of d(CG)$_3$ were not fitted well because of its very low B–Z transition activity (meaning $K_{BZ,1} << 1$). These results suggest that the intermolecular H-bonding interaction of K56 with the phosphate backbone of Z-DNA significantly contributes not only to DNA binding of caZα$_{PKZ}$ but also to its B–Z transition activity.

The hydrogen exchange rate constants (k_{ex}) for the imino protons of both free and caZα$_{PKZ}$-bound dT(CG)$_3$ and d(CG)$_3$ were determined at 35°C. The G2b and G4b protons of free dT(CG)$_3$ have significantly smaller k_{ex} values compared to those of free d(CG)$_3$ (Figure 6C and D), in-

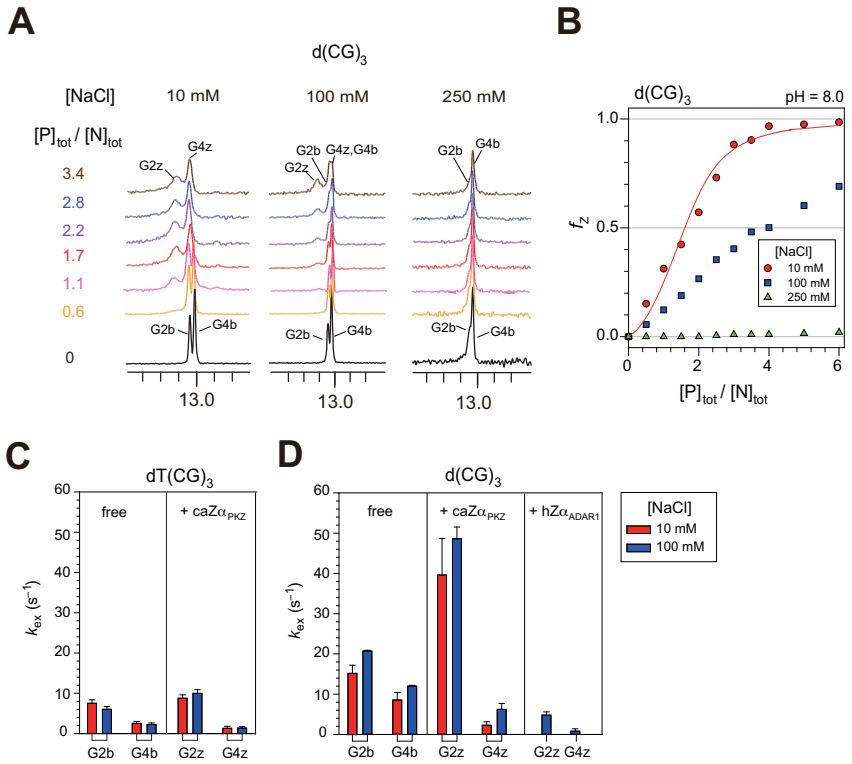

Figure 6. Contribution of H-bonding interaction of K56 with Z-DNA phosphate to B–Z transition. (**A**) 1D imino proton spectra of $d(CG)_3$ at 35°C upon titration with $caZ\alpha_{PKZ}$ in NMR buffer (pH = 8.0) containing 10 (left), 100 (middle) or 250 mM NaCl (right). The resonances from B-form are labeled as G2b and G4b and those from Z-form are labeled as G2z and G4z. (**B**) Relative Z-DNA populations (f_Z) of $d(CG)_3$ induced by $caZ\alpha_{PKZ}$ in NMR buffer containing 10 (red circle), 100 (blue square) or 250 mM NaCl (green triangle) as a function of $[P]_{tot}/[N]_{tot}$ ratio. Solid lines are the best fit to Equation (8). (**C**) The exchange rate constants (k_{ex}) of the imino protons of the free $dT(CG)_3$ (left) and $caZ\alpha_{PKZ}$–$dT(CG)_3$ (right, $[P]_{tot}/[N]_{tot} = 3.4$) at 35°C. (**D**) The k_{ex} of the imino protons of the free $d(CG)_3$ (left), $caZ\alpha_{PKZ}$–$d(CG)_3$, (middle, $[P]_{tot}/[N]_{tot} = 6.0$) and $hZ\alpha_{ADAR1}$–$d(CG)_3$, (right, previous data (11)) at 35°C.

dicating that the flanking T residue of $dT(CG)_3$ leads to greater stabilization of the central G·C base-pairs. In the $caZ\alpha_{PKZ}$–$dT(CG)_3$ complex, the k_{ex} of G4z are significantly smaller than those of free $dT(CG)_3$, whereas the G2z imino protons have slightly larger k_{ex} than the corresponding G2b protons (Figure 6C). Surprisingly, the G2z in the $caZ\alpha_{PKZ}$–$d(CG)_3$ complex has significantly larger k_{ex} than in the $caZ\alpha_{PKZ}$–$dT(CG)_3$ complex (Figure 6D), consistent with severe line-broadening of the G2z imino resonance (Figure 6A). These results indicate that the intermolecular H-bonding interaction of K56 plays an important role in stabilization of the G2·C5 base-pair in Z-DNA.

DISCUSSION

The $caZ\alpha_{PKZ}$ protein requires low salt concentration for full B–Z transition activity, although its overall structure and interactions with Z-DNA are similar to other ZBPs. It has been reported that the typical intracellular salt concentration of fresh water fish is maintained at as few as 10 mM (34,35), and goldfish showed low salinity tolerance (<20 ppt) (36). Thus the salt-dependent B–Z transition activity of $caZ\alpha_{PKZ}$ is thought to reflect the natural environmental conditions of goldfish. We have undertaken a structural analysis of protein–DNA interactions during B–Z transition of a 6-bp DNA by $caZ\alpha_{PKZ}$, in order to understand the salt-dependency of ZBP activity. The NMR chemical shift perturbation (Supplementary Figure S1) and crystal structure analyses (10) can only illustrate the interactions of ZBP with Z-DNA in the final $caZ\alpha_{PKZ}$–Z-DNA (**ZP_2**) complex. However, by applying global analysis on the titration curves, we are able to provide structural information on $caZ\alpha_{PKZ}$ not only in the Z-DNA binding complex but also in the B-DNA binding complex that is the first intermediate structure in the B–Z transition pathway (Supplementary Figure S3). Global analysis gave the K_d of $caZ\alpha_{PKZ}$ for the **BP** (28 nM) and **ZP_2** complexes (345 nM) under 10 mM NaCl condition (Table 2), which have orders of magnitude similar to the previous K_d (851 nM) determined by bio-layer interferometry (10). The values of $k_{on,ZP}$ (1.96×10^9 $M^{-1}s^{-1}$) and $k_{off,ZP2}$ (675 s^{-1}), which are supported by fast exchange behavior in the $^1H/^{15}N$-HSQC spectra during titration (Supplementary Figure S2), are consistent with the association process of 10^9–10^{10} $M^{-1}s^{-1}$ reported for protein–nucleic acid interactions (15,37–39). Taken together, we conclude that the analysis of CPMG data combined with global fitting of titration curves is the most effective method to estimate accurate dissociation constants as well as dissociation/association rate constants in a multi-site protein–DNA binding system including conformational changes of DNA and/or proteins.

The increase of [NaCl] from 10 to 100 mM exhibits a larger effect on the $k_{on,ZP}$ (13-fold larger) than $k_{off,ZP2}$ (2-

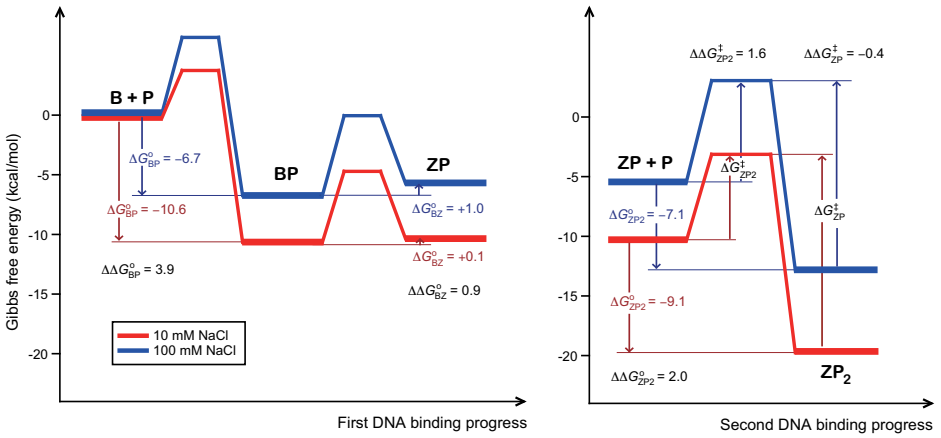

Figure 7. Quantitative description of the energy landscape of the first (lef) and second DNA binding (right) of caZα$_{PKZ}$ at 10 (red) or 100 mM NaCl (blue). Gibbs free energies for the DNA binding and B–Z transition steps were calculated using the equation, $\Delta G^{o} = RT\ln K_{d}$, where R is the gas constant and K_{d} is the dissociation constant for DNA binding ($K_{d,BP}$ or $K_{d,ZP2}$) or $\Delta G^{o} = -RT\ln K_{BZ,1}$, where $K_{BZ,1}$ is the equilibrium constant for B–Z transition. The activation energy difference ($\Delta\Delta G^{\ddagger}_{ZP2}$) for the Z-DNA binding of caZα$_{PKZ}$ between 10 and 100 mM NaCl condition was calculated using the equation, $\Delta\Delta G^{\ddagger}_{ZP2} = \Delta G^{\ddagger}_{ZP2}{}^{100mM} - \Delta G^{\ddagger}_{ZP2}{}^{10mM} = -RT\ln(k_{on,ZP}{}^{100mM}/k_{on,ZP}{}^{10mM})$, where $k_{on,ZP}{}^{10mM}$ and $k_{on,ZP}{}^{100mM}$ are the association rate constants for Z-DNA binding of caZα$_{PKZ}$ at 10 and 100 mM NaCl, respectively.

fold larger), and this resulted in a 25-fold larger $K_{d,ZP2}$ (Table 2). Similar results were observed for the binding of Fyn SH3 domain to substrate peptides (40). The Gibbs free energies for the formation of **ZP$_2$** can be calculated using the equation $\Delta G^{o}{}_{ZP2} = RT\ln K_{d,ZP2}$. The results revealed that the difference between the $\Delta G^{o}{}_{ZP2}$ values at 10 and 100 mM NaCl ($\Delta\Delta G^{o}{}_{ZP2} = \Delta G^{o}{}_{ZP2}{}^{100mM} - \Delta G^{o}{}_{ZP2}{}^{10mM}$) is +2.0 kcal/mol (Figure 7). The activation energy differences for association ($\Delta\Delta G^{\ddagger}_{ZP2}$) and dissociation ($\Delta\Delta G^{\ddagger}_{ZP}$) of the **ZP$_2$** complex can be evaluated using the equations, $\Delta\Delta G^{\ddagger}_{ZP2} = -RT\ln(k_{on,ZP}{}^{100mM}/k_{on,ZP}{}^{10mM})$ and $\Delta\Delta G^{\ddagger}_{ZP} = -RT\ln(k_{off,ZP2}{}^{100mM}/k_{off,ZP2}{}^{10mM})$, respectively. The CPMG data revealed that the $\Delta\Delta G^{\ddagger}_{ZP2}$ value was 1.6 kcal/mol whereas $\Delta\Delta G^{\ddagger}_{ZP}$ was only −0.4 kcal/mol (Figure 7), which could be explained by the structural feature that, in the Z-DNA binding complex, caZα$_{PKZ}$ maintains almost the same backbone conformations regardless of salt concentration (Figure 4D). However, the free form of caZα$_{PKZ}$ shows unusual conformational exchange (Figure 5B), which displays distinct $^{1}H/^{15}N$-HSQC spectra with varying salt concentration (Supplementary Figure S4). This structural feature is consistent with the CPMG data showing that, in spite of a 2-fold larger $k_{off,ZP2}$, the $K_{d,ZP2}$ value increased 25× larger as [NaCl] increased from 10 to 100 mM (Table 2). Thus, our study suggested that increasing the ionic strength more strongly interferes with the association of **ZP** with caZα$_{PKZ}$ via the intermolecular electrostatic interactions (related to $k_{on,ZP}$) rather than the dissociation of **ZP$_2$** (related to $k_{off,ZP2}$).

Surprisingly, we found that the structural features of the B-DNA binding complexes (**BP**) of caZα$_{PKZ}$ at 10 and 100 mM NaCl are completely different from each other (Figure 4D). At 10 mM NaCl, the α3, β1–α2 and β-hairpin regions of caZα$_{PKZ}$ participate in strong intermolecular interactions with B-DNA (Figure 4B). This intermolecular interaction in the **BP** complex is able to provide efficient driving force to cause the B–Z conformational change of DNA. However, as [NaCl] increased to 100 mM, the caZα$_{PKZ}$ binds to B-DNA mainly through the α3 helix, with a partial contribution of the β-hairpin (Figure 4B). Global analysis found that increasing [NaCl] from 10 to 100 mM more significantly reduced the Gibbs free energies for the formation of **BP** with $\Delta\Delta G^{o}{}_{BP}$ of 3.9 kcal/mol, which is 2-fold larger than the $\Delta\Delta G^{o}{}_{ZP2}$ value (Figure 7). It is reported that the activity of nitrogen regulatory protein C can be modulated by mutations or BeF_3^-, which drive the equilibrium toward the active state through destabilizing the inactive state and stabilizing the active state, respectively (41). Assuming that caZα$_{PKZ}$ binds to B-DNA to form a fully active **BP** conformation at low salt concentration, increasing the ionic strength screens the intermolecular electrostatic interactions, which participates in formation of the active **BP** conformation, and then the conformational equilibrium is driven toward the inactive state. As shown in Figure 4E, the ∼25–40% chemical shift movements of caZα$_{PKZ}$ upon B-DNA binding, reflecting a lower population of the active **BP** conformation, can explain the relatively lower B–Z transition activity (4.5-fold smaller $K_{BZ,1}$) (Table 1). Thus, the HSQC spectra of the intermediate **BP** complex derived from our global analysis could be used as a molecular ruler to determine the degree of B–Z transition activity of caZα$_{PKZ}$ (Figure 4E).

The hydrogen exchange data of the imino protons indicates that the G·C base-pairs in the caZα$_{PKZ}$–dT(CG)$_3$ complex are less stable compared to the hZα$_{ADAR1}$–d(CG)$_3$ complex (Figure 6C and D). This might be caused by the lack of H-bonding interaction of caZα$_{PKZ}$ with the C5pG6 phosphate of DNA (Figure 1B), which is provided by the K170 sidechain of hZα$_{ADAR1}$ (8). Under low salt conditions, this H-bonding interaction of ZBP rarely affects the DNA binding as well as B–Z transition. In contrast, the H-bonding of K56 with DNA phosphate contributes to not only stabilization of base-pairs in Z-DNA but also DNA binding and B–Z transition (Figure 6). Because the backbone of the β-hairpin in free caZα$_{PKZ}$ is distinct from that of the complex structure (Figure 2B), this interaction plays

an important role in stabilizing the contact of the β-hairpin with Z-DNA in order to achieve full activity of the ZBP. In $hZ\alpha_{ADAR1}$, both the free and complex forms have similar β-hairpin structures (8,42) and thus this interaction is not crucial for the function of the human protein.

In summary, we have performed a structural analysis of the interaction of ZBP $caZ\alpha_{PKZ}$ with DNA during B–Z transition. The solution structure of free $caZ\alpha_{PKZ}$ revealed that the overall structure is very similar to the $caZ\alpha_{PKZ}$–$dT(CG)_3$ complex while the β-hairpin exhibits the different orientation from the crystal structure. Global analysis of chemical shift perturbations found that increasing [NaCl] from 10 to 100 mM reduced the binding affinity of $caZ\alpha_{PKZ}$ for both B-DNA (600-fold) and Z-DNA (25-fold) and decreased its B–Z transition activity (4.6-fold). Our results suggest that the structure of the intermediate complex formed by $caZ\alpha_{PKZ}$ and B-DNA is modulated by varying salt concentration and thus it could be used as a molecular ruler to determine the degree of B–Z transition.

ACCESSION NUMBERS

The atomic coordinates have been deposited in the Protein Data Bank (PDB ID: 2RVC). Chemical-shift assignments have been deposited in the Biological Magnetic Resonance Bank (BMRM ID: 11595).

SUPPLEMENTARY DATA

Supplementary Data are available at NAR Online.

ACKNOWLEDGEMENTS

We thank the GNU Central Instrument Facility for performing NMR experiments and Melissa Stauffer, of Scientific Editing Solutions, for editing the manuscript. This work is dedicated to the memory of the late Prof. Alexander Rich of Massachusetts Institute of Technology.

FUNDING

National Research Foundation of Korea [2010-0020480, 2013R1A2A2A05003837, 2012R1A4A1027750 (BRL) to J.-H.L.; 2015R1C1A1A02036725 to C.-J.P.] funded by the Korean Government (MSIP); Next-Generation BioGreen 21 Program [SSAC, No. PJ01117701 to J.-H.L.]; Samsung Science and Technology Foundation [SSTF-BA1301-01 to K.K.K]. Funding for open access charge: National Research Foundation of Korea; Gyeongsang National University.
Conflict of interest statement. None declared.

REFERENCES

1. Herbert,A. and Rich,A. (1996) The biology of left-handed Z-DNA. *J. Biol. Chem.*, **271**, 11595–11598.
2. Herbert,A. and Rich,A. (1999) Left-handed Z-DNA: structure and function. *Genetica*, **106**, 37–47.
3. Rich,A. and Zhang,S. (2003) Z-DNA: the long road to biological function. *Nat. Rev. Genet.*, **4**, 566–572.
4. Herbert,A., Alfken,J., Kim,Y.G., Mian,I.S., Nishikura,K. and Rich,A. (1997) A Z-DNA binding domain present in the human editing enzyme, double-stranded RNA adenosine deaminase. *Proc. Natl. Acad. Sci. U.S.A.*, **94**, 8421–8426.
5. Schwartz,T., Behlke,J., Lowenhaupt,K., Heinemann,U. and Rich,A. (2001) Structure of the DLM-1-Z-DNA complex reveals a conserved family of Z-DNA-binding proteins. *Nat. Struct. Biol.*, **8**, 761–765.
6. Kim,Y.-G., Muralinath,M., Brandt,T., Pearcy,M., Hauns,K., Lowenhaupt,K., Jacobs,B.L. and Rich,A. (2003) A role for Z-DNA binding in vaccinia virus pathogenesis. *Proc. Natl. Acad. Sci. U.S.A.*, **100**, 6974–6979.
7. Rothenburg,S., Deigendesch,N., Dittmar,K., Koch-Nolte,F., Haag,F., Lowenhaupt,K. and Rich,A. (2005) A PKR-like eukaryotic initiation factor 2α kinase from zebrafish contains Z-DNA binding domains instead of dsRNA binding domains. *Proc. Natl. Acad. Sci. U.S.A.*, **102**, 1602–1607.
8. Schwartz,T., Rould,M.A., Lowenhaupt,K., Herbert,A. and Rich,A. (1999) Crystal structure of the Zα domain of the human editing enzyme ADAR1 bound to left-handed Z-DNA. *Science*, **284**, 1841–1845.
9. Ha,S.C., Lokanath,N.K., Van Quyen,D., Wu,C.A., Lowenhaupt,K., Rich,A., Kim,Y.G. and Kim,K.K. (2004) A poxvirus protein forms a complex with left-handed Z-DNA: crystal structure of a Yatapoxvirus Zα bound to DNA. *Proc. Natl. Acad. Sci. U.S.A.*, **101**, 14367–14372.
10. Kim,D., Hur,J., Park,K., Bae,S., Shin,D., Ha,S.C., Hwang,H.Y., Hohng,S., Lee,J.H., Lee,S. *et al.* (2014) Distinct Z-DNA binding mode of a PKR-like protein kinase containing a Z-DNA binding domain (PKZ). *Nucleic Acids Res.*, **42**, 5937–5948.
11. Kang,Y.-M., Bang,J., Lee,E.-H., Ahn,H.-C., Seo,Y.-J., Kim,K.K., Kim,Y.-G., Choi,B.-S. and Lee,J.-H. (2009) NMR spectroscopic elucidation of the B-Z transition of a DNA double helix induced by the Zα domain of human ADAR1. *J. Am. Chem. Soc.*, **131**, 11485–11491.
12. Seo,Y.-J., Ahn,H.-C., Lee,E.-H., Bang,J., Kang,Y.-M., Kim,H.-E., Lee,Y.-M., Kim,K., Choi,B.-S. and Lee,J.-H. (2010) Sequence discrimination of the Zα domain of human ADAR1 during B-Z transition of DNA duplexes. *FEBS Lett.*, **584**, 4344–4350.
13. Lee,E.-H., Seo,Y.-J., Ahn,H.-C., Kang,Y.-M., Kim,H.-E., Lee,Y.-M., Choi,B.-S. and Lee,J.-H. (2010) NMR study of hydrogen exchange during the B-Z transition of a DNA duplex induced by the Zα domains of yatapoxvirus E3L. *FEBS Lett.*, **584**, 4453–4457.
14. Fielding,L. (2007) NMR methods for the determination of protein–ligand dissociation constants. *Prog. NMR Spectrosc.*, **51**, 219–242.
15. Arai,M., Ferreon,J.C. and Wright,P.E. (2012) Quantitative analysis of multisite protein-ligand interactions by NMR: binding of intrinsically disordered p53 transactivation subdomains with the TAZ2 domain of CBP. *J. Am. Chem. Soc.*, **134**, 3792–3803.
16. Hu,C.Y., Zhang,Y.B., Huang,G.P., Zhang,Q.Y. and Gui,J.F. (2004) Molecular cloning and characterisation of a fish PKR-like gene from cultured CAB cells induced by UV-inactivated virus. *Fish Shellfish Immunol.*, **17**, 353–366.
17. Su,J., Zhu,Z. and Wang,Y. (2008) Molecular cloning, characterization and expression analysis of the PKZ gene in rare minnow Gobiocypris rarus. *Fish Shellfish Immunol.*, **25**, 106–113.
18. Bergan,V., Jagus,R., Lauksund,S., Kileng,Ø. and Robertsen,B. (2008) The Atlantic salmon Z-DNA binding protein kinase phosphorylates translation initiation factor 2α and constitutes a unique orthologue to the mammalian dsRNA-activated protein kinase R. *FEBS J.*, **275**, 184–197.
19. Delaglio,F., Grzesiek,S., Vuister,G.W., Zhu,G., Pfeifer,J. and Bax,A. (1995) NMRPipe: a multidimensional spectral processing system based on UNIX pipes. *J. Biomol. NMR*, **6**, 277–293.
20. Goddard,T.D. and Kneller,D.G. (2003) *SPARKY 3*. University of California, San Francisco, CA.
21. Shen,Y., Delaglio,F., Cornilescu,G. and Bax,A. (2009) TALOS+: a hybrid method for predicting protein backbone torsion angles from NMR chemical shifts. *J. Biomol. NMR*, **44**, 213–223.
22. Wishart,D.S. and Sykes,B.D. (1994) The ^{13}C chemical-shift index: a simple method for the identification of protein secondary structure using ^{13}C chemical-shift data. *J. Biomol. NMR*, **4**, 171–180.
23. Brünger,A.T., Adams,P.D., Clore,G.M., DeLano,W.L., Gros,P., Grosse-Kunstleve,R.W., Jiang,J.S., Kuszewski,J., Nilges,M., Pannu,N.S. *et al.* (1998) Crystallography & NMR system: a new software suite for macromolecular structure determination. *Acta Crystallogr. D Biol. Crystallogr.*, **54**, 905–921.
24. Nederveen,A.J., Doreleijers,J.F., Vranken,W., Miller,Z., Spronk,C.A., Nabuurs,S.B., Güntert,P., Livny,M., Markley,J.L., Nilges,M. *et al.*

(2005) RECOORD: a recalculated coordinate database of 500+ proteins from the PDB using restraints from the BioMagResBank. *Proteins*, **59**, 662–672.
25. Brunger,A.T. (2007) Version 1.2 of the Crystallography and NMR system. *Nat. Protoc.*, **2**, 2728–2733.
26. Laskowski,R.A., Rullmannn,J.A., MacArthur,M.W., Kaptein,R. and Thornton,J.M. (1996) AQUA and PROCHECK-NMR: programs for checking the quality of protein structures solved by NMR. *J. Biomol. NMR*, **8**, 477–486.
27. Luz,Z. and Meiboom,S. (1963) Nuclear magnetic resonance study of the protolysis of trimethylammonium ion in aqueous solution: order of the reaction with respect to solvent. *J. Chem. Phys.*, **39**, 366–370.
28. Villali,J., Pontiggia,F., Clarkson,M.W., Hagan,M.F. and Kern,D. (2014) Evidence against the 'Y-T coupling' mechanism of activation in the response reculator NtrC. *J. Mol. Biol.*, **426**, 1554–1567.
29. Wang,Z.-X. and Jiang,R.-F. (1996) A novel two-site binding equation presented in terms of the total ligand concentration. *FEBS Lett.*, **492**, 245–249.
30. Gueron,M. and Leroy,J.L. (1995) Studies of base pair kinetics by NMR measurement of proton exchange. *Methods Enzymol.*, **261**, 383–413.
31. Lee,J.-H. and Pardi,A. (2007) Thermodynamics and kinetics for base-pair opening in the P1 duplex of the *Tetrahymena* group I ribozyme. *Nucleic Acids Res.*, **35**, 2965–2974.
32. Lee,J.-H., Jucker,F. and Pardi,A. (2008) Imino proton exchange rates imply an induced-fit binding mechanism for the $VEGF_{165}$-targeting aptamer, Macugen. *FEBS Lett.*, **582**, 1835–1839.
33. Palmer,A.G., Kroenke,C.D. and Loria,J.P. (2001) Nuclear magnetic resonance methods for quantifying microsecond-to-millisecond motions in biological macromolecules. *Methods Enzymol.*, **339**, 204–238.
34. Morgan,I., Potts,W. and Oates,K. (1994) Intracellular ion concentrations in branchial epithelial cells of brown trout (*Salmo trutta L.*) determined by X-ray microanalysis. *J. Exp. Biol.*, **194**, 139–151.
35. Li,J., Eygensteyn,J., Lock,R., Bonga,S. and Flik,G. (1997) Na^+ and Ca^{2+} homeostatic mechanisms in isolated chloride cells of the teleost Oreochromis mossambicus analysed by confocal laser scanning microscopy. *J. Exp. Biol.*, **200**, 1499–1508.
36. Schofield,P.J., Brown,M.E. and Fuller,P.F. (2006) Salinity tolerance of goldfish,*Carassius auratus*, a non-native fish in the United States. *Fla. Sci.*, **69**, 258–268.
37. Winter,R.B., Berg,O.G. and von Hippel,P.H. (1981) Diffusion-driven mechanisms of protein translocation on nucleic acids. 3. The *Escherichia coli* lac repressor-operator interaction: kinetic measurements and conclusions. *Biochemistry*, **20**, 6961–6977.
38. Park,C. and Raines,R.T. (2001) Quantitative analysis of the effect of salt concentration on enzymatic catalysis. *J. Am. Chem. Soc.*, **123**, 11472–11479.
39. Korennykh,A.V., Piccirilli,J.A. and Correll,C.C. (2006) The electrostatic character of the ribosomal surface enables extraordinarily rapid target location by ribotoxins. *Nat. Struct. Mol. Biol.*, **13**, 436–443.
40. Meneses,E. and Mittermaier,A. (2014) Electrostatic interactions in the binding pathway of a transient protein complex studied by NMR and isothermal titration calorimetry. *J. Biol. Chem.*, **289**, 27911–27923.
41. Gardino,A.K., Villali,J., Kivenson,A., Lei,M., Liu,C.F., Steindel,P., Eisenmesser,E.Z., Labeikovsky,W., Wolf-Watz,M., Clarkson,M.W. *et al.* (2009) Transient non-native hydrogen bonds promote activation of a signaling protein. *Cell*, **139**, 1109–1118.
42. Schade,M., Turner,C.J., Kuhne,R., Schmieder,P., Lowenhaupt,K., Herbert,A., Rich,A. and Oschkinat,H. (1999) The solution structure of the Zα domain of the human RNA editing enzyme ADAR1 reveals a prepositioned binding surface for Z-DNA. *Proc. Natl. Acad. Sci. U.S.A.*, **96**, 12465–12470.